JACS
JOURNAL OF THE AMERICAN CHEMICAL SOCIETY
Article
pubs.acs.org/JACS

Ionic Conductor with High Conductivity as Single-Component Electrolyte for Efficient Solid-State Dye-Sensitized Solar Cells

Hong Wang, Juan Li, Feng Gong, Gang Zhou, and Zhong-Sheng Wang*

Department of Chemistry, Lab of Advanced Materials, Collaborative Innovation Center of Chemistry for Energy Materials, Fudan University, Songhu Road 2205, 200438 Shanghai, P. R. China

Supporting Information

ABSTRACT: Imidazolium iodide is an often used component in iodine-based dye-sensitized solar cells (DSSCs), but it cannot operate an efficient DSSC in the absence of iodine due to its low conductivity. For this study, lamellar solid iodide salts of imidazolium or piperidinium with an N-substituted propargyl group have been prepared and applied in solid-state DSSCs. Owing to the high conductivity arising from the lamellar structure, these solid-state ionic conductors can be used as single-component solid electrolytes to operate solid-state DSSCs efficiently without any additives in the electrolyte and post-treatments on the dye-loaded TiO_2 films. With a propargyl group attached to the imidazolium ring, the conductivity is enhanced by about 4×10^4-fold as compared to the alkyl-substituted imidazolium iodide. Solid-state DSSC with the 1-propargyl-3-methylimidazolium iodide as the single-component solid-state electrolyte has achieved a light-to-electricity power conversion efficiency of 6.3% under illumination of simulated AM1.5G solar light (100 mW cm^{-2}), which also exhibits good long-term stability under continuous 1 sun soaking for 1500 h. This finding paves the way for development of high-conductivity single-component solid electrolytes for use in efficient solid-state DSSCs.

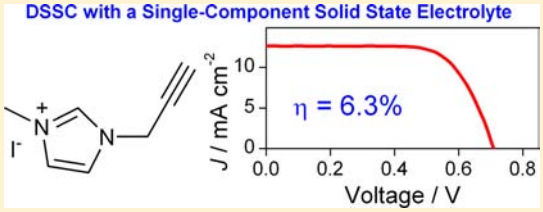

INTRODUCTION

Dye-sensitized solar cells (DSSCs), which have emerged as one of the most promising photovoltaic devices, have been studied extensively due to their respectable power conversion efficiency, facile fabrication processes, and potential low cost.[1] The typical DSSC is, in its original form, composed of dye-sensitized nanocrystalline TiO_2 film as the working electrode, a Pt-coated conductive glass as the counter electrode, and the redox couple I^-/I_3^- in a volatile organic solvent as the electrolyte. Although power conversion efficiency over 12% has been achieved for DSSCs with a volatile organic liquid electrolyte,[1d] DSSCs containing liquid electrolyte are limited for outdoor applications in view of the need for robust encapsulation of the volatile organic liquid. For this reason, considerable efforts have been made to replace the liquid electrolyte with solid-state electrolytes, such as p-type inorganic semiconductors (CuI, CuSCN, etc.),[2] organic hole-transporting materials,[3−5] and ionic conductors.[6,7]

Among the solid-state electrolytes, ionic conductors based on imidazolium iodides and their polymers are promising candidates for application in solid-state DSSCs (ssDSSCs). As the ionic conductors themselves usually suffer from low conductivity, the ssDSSCs based on them without any additives in the solid electrolyte or post-treatments on the dye-sensitized film cannot work or are much less efficient than those with additives in the solid electrolyte or post-treatments on the dye-sensitized film. Doping of iodine and LiI into ionic conductors has been confirmed to improve the conductivity and photovoltaic performance significantly according to our previous report.[8] Unfortunately, the presence of iodine or triiodide brings about disadvantages, such as charge recombination and incident light filtering by iodine below 500 nm, which can decrease photovoltaic performance.[9] In addition, multiple components of the solid electrolyte inevitably bring about complexity of the device, which is not propitious for performance optimization, mechanism analysis, and mass production. Additives are also required for efficient ssDSSCs based on hole-transporting materials. For example, an additive such as $(p\text{-}BrC_6H_4)_3NSbCl_6$ or Co(III) complexes was doped in 2,2′,7,7′-tetrakis(*N*,*N*-di-*p*-methoxyphenylamine)-9,9′-spirobifluorene (spiro-MeOTAD)[5,10] and $LiN(CF_3SO_2)_2$ was doped in PEDOT[11] to improve the conductivity and thus enhance the solar cell performance. The perplexing components raise the cost of ssDSSC and may influence the long-term stability due to some unknown side reactions. On the basis of the above points, it is much desired to develop a single-component solid-state electrolyte with high conductivity for use in stable and efficient ssDSSCs.

High conductivity is the requirement for a single-component solid-state electrolyte to operate an efficient ssDSSC. For imidazolium (or piperidinium) iodide salts, conductivity can be attributed to charge transfer along the polyiodide chain according to the relay-type Grotthus mechanism.[12] A lamellar structure[13] is favorable for such charge transfer and expected to yield high conductivity. Herein, we designed and synthesized iodide salts of imidazolium or piperidinium with a pendent propargyl group (PMIm and PMPi, Figure 1a) for applications

Received: February 20, 2013
Published: August 2, 2013

   dx.doi.org/10.1021/ja401827w | J. Am. Chem. Soc. 2013, 135, 12627−12633

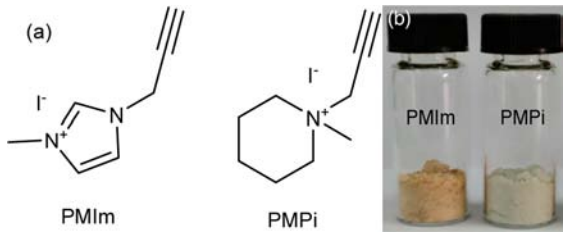

Figure 1. Structures of the propargyl-functionalized ionic conductors (a) and their photograph (b).

in ssDSSCs. As compared to the alkyl-substituted imidazolium iodide, introduction of unsaturated propargyl group to the imidazolium ring enhanced the conductivity by more than 4 orders. As a consequence, the propargyl-functionalized ionic conductor itself can be used directly as a single-component solid-state electrolyte for ssDSSCs, which can perform efficiently without any additives in the electrolyte and any post-treatments on the dye-loaded TiO_2 films. This single-component solid-state electrolyte-based ssDSSC with an organic dye (MK2, Figure S1, Supporting Information)[14] achieved power conversion efficiency of 6.3% under simulated AM1.5G illumination (100 mW cm^{-2}) and exhibited good long-term stability under continuous 1 sun soaking for 1500 h.

EXPERIMENTAL SECTION

Materials and Reagents. Imidazole, sodium, iodomethane, and piperidine were purchased from J&K Chemical Ltd., China. Organic solvents used in this work were purified using the standard processes. Transparent conductive glass (F-doped SnO_2, FTO, 15 Ω/square, transmittance of 85%, Nippon Sheet Glass Co., Japan) was used as the substrate for fabrication of TiO_2 thin film electrode. Dye sensitizer (MK2, Figure S1, Supporting Information) used in this work was synthesized according to the literature method.[14] Synthetic routes of the ionic conductors are described in Scheme 1.

Scheme 1. Synthetic Routes of the Ionic Conductors

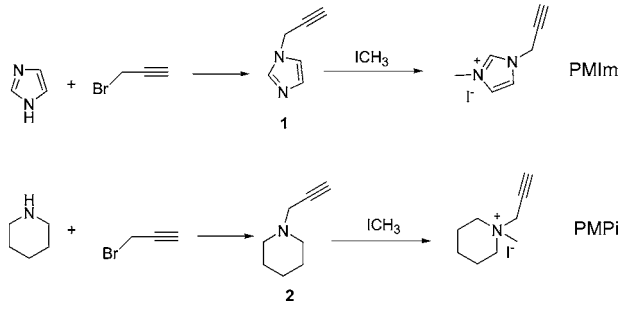

Characterization. Propargyl-functionalized ionic conductors were characterized by ^1H NMR (Varian 400 MHz NMR spectrometer) and elemental analysis (Vario EL3, Germany). Mass spectra were obtained on an HP-5988A spectrometer by direct inlet at 70 eV. Thermogravimetric (TG) analysis was performed on a TG-DTA 2000S system (Mac Sciences Co. Ltd., Yokohama, Japan) at a heating rate of 10 °C min^{-1}. Differential scanning calorimetry (DSC) was performed on a DSC 822e thermal analysis system (Mettler Toledo Instruments Inc., Switzerland) with nitrogen gas as purge (80 mL min^{-1}) at a heating rate of 5 °C min^{-1} in a temperature range of 25–150 °C. The morphology of the product was observed on a field-emitting scanning electron microscope (FESEM, S-4800, Hitachi, Japan). X-ray diffraction (XRD) patterns for the ionic conductors were measured on a X-ray powder diffractometer (D8 Advance, Bruker, Germany) with Cu Kα radiation (λ = 0.154 nm). Raman spectra were recorded using a Dilor LabRam-1B spectrometer, operating at a resolution of 1 cm^{-1}. The Spectra Physics model 164 argon-ion laser was operated at 632.8 nm with about 6 mW of power. UV–vis absorption spectra were scanned on a UV–vis–NIR spectrophotometer (Shimadzu UV-2550) in transmission mode. Solid-state electrolytes were sandwiched in dummy cells between two identical Pt electrodes, which were used for measurements of electrochemical impedance spectroscopy (EIS) in a frequency range from 1 Hz to 1 MHz and cyclic voltammetry (CV) on an electrochemical workstation (Zahner XPOT, Germany).

Fabrication and Photovoltaic Measurements of ssDSSCs. TiO_2 films (10 μm) composed of a 6 μm nanoparticle (20 nm) layer in direct contact with the FTO substrate and 4 μm light scattering particle (80% 20 nm TiO_2 + 20% 100 nm TiO_2) layer[15] were fabricated with a screen-printing method and used in this study. Films were sintered at 500 °C for 2 h to achieve good necking of neighboring TiO_2 particles. Film thickness was measured with a surface profiler (Veeco Dektak 150, USA). Sintered films were then treated with 0.05 M $TiCl_4$ aqueous solution at 70 °C for 30 min followed by heating at 450 °C for 30 min. When TiO_2 electrodes were allowed to cool to about 120 °C, electrodes were immersed into the MK2 dye solution (0.3 mM in toluene) for 24 h at room temperature for complete dye adsorption. Dye-loaded TiO_2 film as the working electrode and the Pt-coated FTO as the counter electrode were separated by a hot-melt Surlyn film (30 μm) and sealed together by pressing them under heat. The methanol solution of the solid electrolyte was injected repeatedly into the interspace between the working and the counter electrodes from the two holes predrilled on the back of the counter electrode and dried on a hot plate at 50 °C until the TiO_2 porous film was filled with the solid-state electrolyte. The cell was further dried in a vacuum oven at 50 °C for 2 days to completely remove the residual methanol and form a compact solid electrolyte layer for efficient charge transfer through the solid ionic conductor. Finally, the two holes were sealed with a Surlyn film covered with a thin glass slide under heat. The working performance of DSSC was tested by recording the current density–voltage (J–V) curves with a Keithley 2400 Source Meter (Oriel) under illumination of simulated AM1.5G solar light coming from an AAA solar simulator (Newport-94043A) equipped with a Xe lamp (450 W) and an AM1.5G filter. Light intensity was calibrated using a standard Si solar cell (Newport 91150) equipped with a KG-5 filter. Action spectra of incident monochromatic photon-to-electron conversion efficiency (IPCE) as a function of wavelength were obtained on an Oriel-74125 system (Oriel Instruments). The intensity of incident monochromatic light was measured with a Si detector (Oriel-71640). A black mask with an aperture area of 0.2304 cm^2 was used during measurement to avoid stray light completely.

Synthesis of Ionic Conductors. Absolute dry methanol (100 mL) and sodium (4.6 g, 0.2 mol) were charged into a 250 mL three-necked flask equipped with a condensing tube and stirred at room temperature for 2 h. Then, imidazole (13.6 g, 0.2 mol) was added to the above mixture under nitrogen, which was heated to 50 °C. After stirring for 1 h, propargyl bromide (11.9 g, 0.1 mol) was added dropwise to the above system. The reaction was kept at 50 °C for an additional 16 h and then allowed to cool down to room temperature. After filtration, the filtrate was collected and the solvent was removed via rotary evaporation until yellow liquid remained. Silica gel chromatography with CH_2Cl_2:CH_3OH (30:1, v:v) as eluent afforded compound **1** with a yield of 63%.

Compound **2** was obtained with the same procedures for compound **1** except that the starting material imidazole was replaced with piperidine. The yield was 65%.

The ionic conductor PMIm was prepared by quaternization of compound **1** with iodomethane, and PMPi was prepared by quaternization of compound **2** with iodomethane (Scheme 1).

Compound **1** (2.0 g, 0.02 mol), 10 mL of methanol, and iodomethane (5.7 g, 0.04 mol) were charged into a 50 mL three-necked flask equipped with a condensing tube and stirred at 50 °C for 48 h. Then, the reaction mixture was reprecipitated in diethyl ether to produce PMIm with a yield of 99%.

dx.doi.org/10.1021/ja401827w | J. Am. Chem. Soc. 2013, 135, 12627–12633

PMPi was obtained with the same procedures as PMIm except compound **1** was replaced with compound **2**. The yield was 99%.

The structures for compound **1** and **2** and the two ionic conductors were testified by ^{1}H NMR and ^{13}C NMR (Varian 400 MHz NMR spectrometer) as detailed in the following.

Compound 1. ^{1}H NMR (DMSO-d_6, 400 Hz, δ ppm): 3.46 (s, 1H); 4.89−4.90 (d, 2H); 6.91(s, 1H), 7.19 (s, 1H), 7.67 (s, 1H). ^{13}C NMR (DMSO-d_6, 50 MHz, δ ppm): 36.1, 76.8, 79.3, 120.0, 129.3, 137.7.

Compound 2. ^{1}H NMR ($CDCl_3$, 400 Hz, δ ppm): 1.37 (s, 2H), 1.52−1.58 (m, 4H), 2.17−2.18 (t, 1H), 2.4 (s, 4H), 3.20−3.21 (d, 2H). ^{13}C NMR ($CDCl_3$, 50 MHz, δ ppm): 79.4, 73.0, 53.3, 47.8, 26.0, 24.0.

Structures of the final products were characterized by ^{1}H NMR, elemental analysis, ESI-MS, and FT-IR (Shimadzu IRAffinity-1) as detailed in the following.

PMIm. ^{1}H NMR (D_2O, 400 Hz, δ ppm): 2.9−3.0 (t, 1H); 3.79 (s, 3H,); 4.95−4.96 (d, 2H), 7.35 (s, 1H); 7.46 (s, 1H); 8.78 (s, 1H). Anal. Calcd for $C_7H_9N_2I$: C, 33.89; H, 3.66; N, 11.29. Found: C, 33.50; H, 3.61; N, 10.86. ESI-MS (m/z): calcd for $C_7H_9N_2^+$, 121.08; found, 121.07. C≡C stretching and C≡C−H stretching IR bands were observed at 2124 and 3188 cm^{-1}, respectively (Figure S2, Supporting Information).

PMPi. ^{1}H NMR (D_2O, 400 Hz, δ ppm): 1.44−1.50 (m, 2H), 1.69−1.70 (d, 4H), 2.97 (s, 3H), 3.02 (s, 1H), 3.21−3.34 (m, 4H), 4.08 (d, 2H). Anal. Calcd for $C_9H_{16}NI$: C, 40.77; H, 6.08; N, 5.28. Found: C, 40.44; H, 6.08; N, 5.67. ESI-MS (m/z): calcd for $C_9H_{16}N^+$, 138.13; found, 138.09. C≡C stretching and C≡C−H stretching IR bands were observed at 2124 and 3181 cm^{-1}, respectively (Figure S2, Supporting Information).

RESULTS AND DISCUSSION

The facile synthetic route for PMIm and PMPi includes only two simple steps from inexpensive commercially available materials, as detailed in the Experimental Section. IR stretching bands for C≡C and C≡C−H are clearly observed for PMIm and PMPi (Figure S2, Supporting Information), indicating that the propargyl group is linked to the imidazolium or piperidinium ring. Further characterization via ^{1}H NMR (see Supporting Information), elemental analysis, and ESI-MS confirm that the obtained products have the structures shown in Figure 1a. As-prepared propargyl-functionalized ionic conductors are solid state (Figure 1b) below 80 °C and have good solubility in common organic solvents such as methanol and ethanol, which is advantageous to solution processing for solid-state electrolyte filling in ssDSSCs.

Figure 2a shows the TG curves for the two propargyl-functionalized ionic conductors. The starting decomposition temperatures, at which the decomposition of these propargyl-functionalized ionic conductors begins, have been determined by TG analysis. PMIm and PMPi start to decompose at 245 and 224 °C, respectively. The TG results indicate that these propargyl-functionalized ionic conductors have very good thermal stability below 200 °C, making them good candidates for outdoor applications of solar cells. Figure 2b displays DSC curves of the two ionic conductors. One sharp endothermic peak, where the propargyl-functionalized ionic conductor undergoes phase transition from solid to liquid, was observed for each propargyl-functionalized ionic conductor. Melting points were determined to be 100 and 80 °C for PMIm and PMPi, respectively, using the peak temperature of DSC curves. As compared to 1-methyl-3-propylimidazolium iodide (liquid), replacement of propyl with a propargyl group (forming PMIm) raised the melting point significantly due to the rigidity of the carbon−carbon triple bond. The high melting points for these propargyl-functionalized ionic conductors enable them to remain in the solid state when applied outdoors.

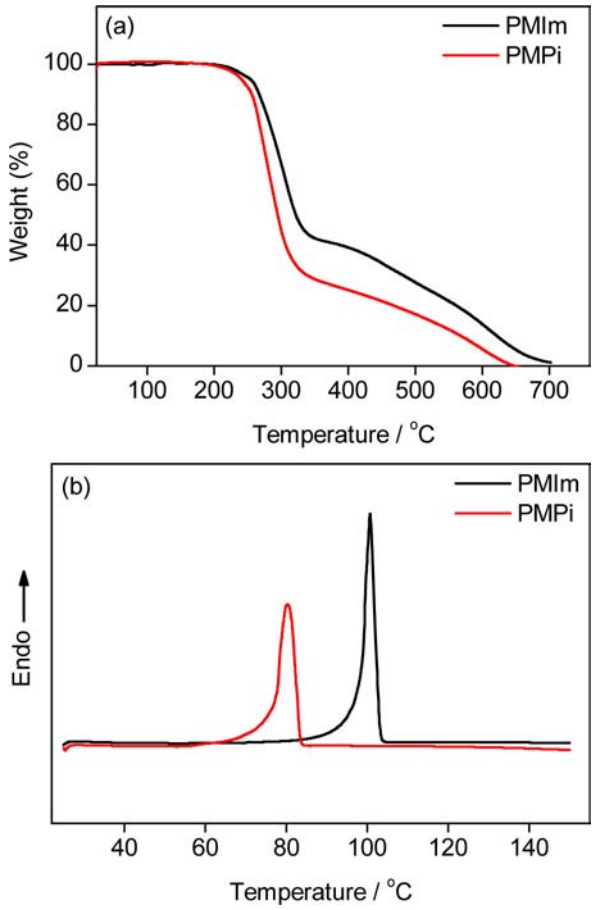

Figure 2. TGA curves (a) and DSC curves (b) of the as-prepared propargyl-functionalized ionic conductors.

Figure 3 displays the FESEM images for these propargyl-functionalized ionic conductors. Films obtained from drop casting methanol solutions onto FTO glass exhibited lamellar structures. It is noted that we cannot provide solid proof for the two-dimensional lamellar structure so far. A single-crystal structure is useful to clarify formation of the lamellar structure, but unfortunately we failed to get single crystals, though we tried many times. As 1-propargyl-3-methylimidazolium iodide is similar to 1-propargyl-3-methylimidazolium bromide, whose single-crystal structure has already been reported,[13] we attribute the lamellar structure to the alternating packing of cations and anions dominated by the attractive Coulomb forces and hydrogen bonding. The iodide anion is connected to different cations by hydrogen bonding, forming a three-dimensional network.[13]

XRD measurements provide insight into the molecular packing arrangement of the ionic conductors. Figure 4 shows the XRD patterns for these ionic conductors, where Bragg peaks are clearly observed at 11.7° and 9.6° for PMIm and PMPi, respectively. The spacing (d) between planes in the atomic lattice can be calculated using Bragg's law

$$2d \sin \theta = n\lambda \quad (1)$$

where λ is the wavelength (= 0.154 nm) of the incident beam, θ is the angle between the incident ray and the scattering plane, and n is an integer. Interlayer distances of 7.6 and 9.2 Å for PMIm and PMPi, respectively, are obtained according to eq 1. PMPi showed a larger interlayer distance due to the twisting of the piperidinium ring, while PMIm showed a smaller interlayer

dx.doi.org/10.1021/ja401827w | J. Am. Chem. Soc. 2013, 135, 12627−12633

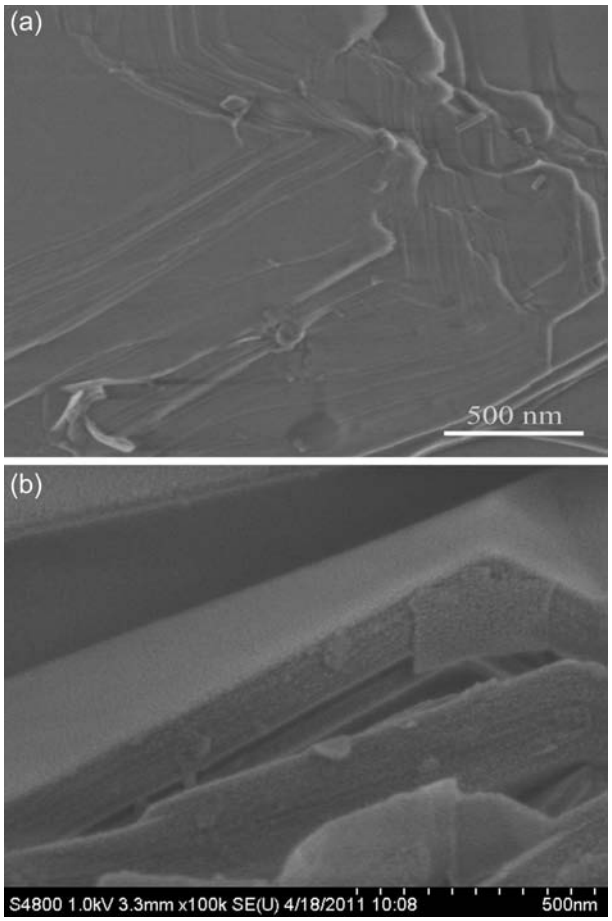

Figure 3. FESEM images of PMIm (a) and PMPi (b).

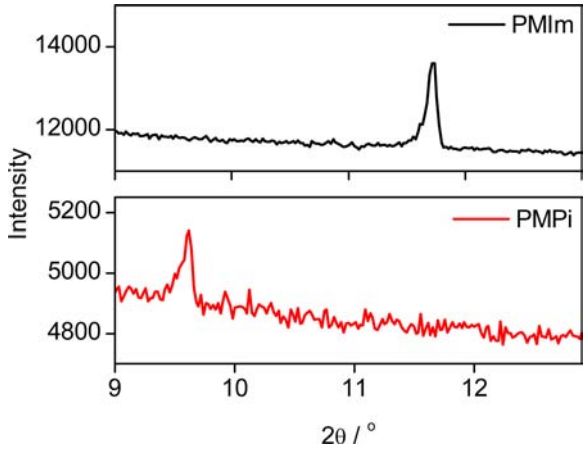

Figure 4. XRD patterns of the propargyl-functionalized ionic conductors.

distance due to the planarity of the imidazolium ring. The layer structured feature of these propargyl-functionalized ionic conductors is beneficial to fast charge transport along the polyiodide chain. As compared to PMPi, PMIm exhibited a stronger Bragg peak, suggesting that the latter has better crystallinity than the former.

Table 1 lists the conductivity for PMIm and PMPi. The conductivity at room temperature for PMIm was higher than that for PMPi. This can be explained by the smaller interlayer distance and better crystallinity for PMIm as compared to

Table 1. Conductivity for the Propargyl-Functionalized Ionic Conductors and Photovoltaic Performance Parameters of ssDSSCs with Them as Solid-State Electrolytes

solid electrolyte	σ/mS cm^{-1}	J_{sc}/mA cm^{-2}	V_{oc}/V	FF	η/%
PMIm	40	12.65	0.71	0.70	6.3
PMPi	9	5.21	0.66	0.65	2.2
DMPImI	1.0×10^{-3}	0	0	0	0

PMPi, revealed by the XRD peak position and intensity. Impressively, the conductivity of PMIm was as high as 40 mS cm^{-1} at room temperature, which was even higher than that (25 mS cm^{-1}) for the solution of 0.4 M LiI + 0.04 M I_2 in acetonitrile.[16] To emphasize the effect of the propargyl group on the conductivity, we compared PMIm with 1,2-dimethyl-3-propylimidazolium iodide (DMPImI, solid state at room temperature). It is seen from Table 1 that introduction of propargyl to the imidazolium ring enhanced the conductivity by 40 000-fold. This indicates that our molecular design is successful to achieve high conductivity.

The temperature dependence of conductivity for the as-prepared ionic conductors is shown in Figure 5. It can be seen

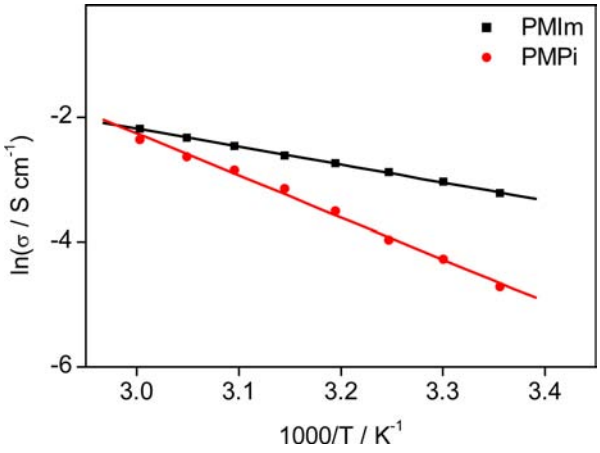

Figure 5. Temperature dependence of the ionic conductivity for the two propargyl-functionalized ionic conductors.

from Figure 5 that conductivity increases with temperature. The data in Figure 5 can be fitted well by the Arrhenius equation[17]

$$\sigma = \sigma_0 \exp(-E_a/kT) \quad (2)$$

where σ_0 is a constant, E_a the activation energy, k Boltzmann's constant, and T the absolute temperature. The linear dependence of ln σ on $1/T$ indicates that the conductivity of these propargyl-functionalized ionic conductors is attributed to ionic conduction, which originates from the charge transfer along the polyiodide chain according to the relay-type Grotthus mechanism.[12] Charge transfer along the polyiodide chain just looks like movements of iodide and triiodide in opposite directions. As reported by Thorsmølle et al.,[18] the Grotthus mechanism can only contribute to ionic charge transport at iodine concentrations above 3.6 M for 1-methyl-3-propylimidazolium iodide. The main reason is that high iodine/iodide packing density can reduce the distance between iodide/polyiodide species, which enhances Grotthus bond exchange ($I^- + I_3^- = I_3^- + I^-$) and thus leads to extraordinarily efficient charge transport.[18] This indicates that Grotthus bond exchange

dx.doi.org/10.1021/ja401827w | J. Am. Chem. Soc. 2013, 135, 12627−12633

depends not only on iodine concentration but also on the original distance between iodides in the absence of iodine. When the original distance between iodides is small enough, the Grotthus mechanism may also contribute to charge transport at low iodine concentration. For PMIm, iodine is present in the solid electrolyte due to contamination, as revealed by the Raman spectrum (Figure S3, Supporting Information), but the amount of iodine or triiodide is very small. The molar ratio of I_3^-/I^- in PMIm is less than 2×10^{-5} as determined by UV–vis absorption spectra (Figure S4, Supporting Information). It is likely that the distance between iodides in PMIm is very small, which makes Grotthus bond exchange efficient even with a trace amount of triiodide. To prove this point, the single-crystal structure of PMIm is needed for further detailed investigation, which will be the focus of our future study.

To investigate the catalytic property of Pt counter electrode on redox reactions in the solid electrolyte, CV of the solid electrolyte in a dummy cell with two identical Pt electrodes is carried out. A pair of redox peaks is observed for both solid electrolytes, as shown in Figure 6, contrasting to liquid redox

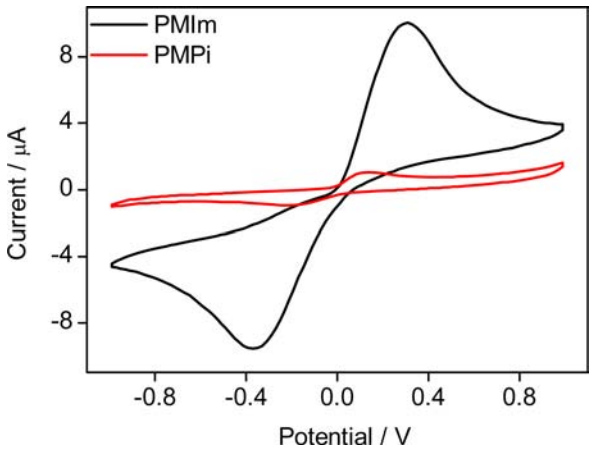

Figure 6. Cyclic voltammograms of PMIm and PMPi sandwiched in dummy cells between two identical Pt electrodes. Scan rate is 100 mV s^{-1}. Area and thickness of the solid electrolyte are 0.36 cm^2 and 30 μm, respectively.

electrolyte solutions that typically display saturation currents when the potential becomes sufficiently positive or negative. For a solid electrolyte sandwiched in a symmetrical cell, the current is likely limited by Grotthus charge exchange rather than diffusion of species as in the solution case. Therefore, when the potential reaches the vicinity of the formal potential for triiodide reduction, reduction begins. As the potential continues to grow more negative, the surface concentration of I_3^- must drop and hence the Grotthus ionic charge exchange increases. As the potential moves past the formal potential, the surface concentration of I_3^- drops nearly to zero, the moving rate of I_3^- to the surface due to Grotthus charge exchange reaches a maximum, and the current decreases. The anodic current appears in a similar way. Therefore, a peaked current–potential curve is observed.

The upper peak in Figure 6 is attributed to oxidation of iodide to triiodide, while the lower peak results from reduction of triiodide to iodide. When the sample was potential scanned for several cycles, a gradual increase in peak currents was observed (Figure S5, Supporting Information). This indicates conversion of iodide to triiodide during CV scan. The magnitude of the peak current is related to the catalytic activity of the Pt electrode and the charge transfer rate along the polyiodide chain. As the Pt electrode is identical for both cases, the larger peak currents for PMIm indicate that the charge transfer rate in PMIm is faster than that in PMPi. Faster charge transfer along the polyiodide chain for PMIm arises from its lamellar structure with a smaller interlayer distance. As a consequence, PMIm exhibits higher conductivity than PMPi.

ssDSSCs with these propargyl-functionalized ionic conductors as single-component solid electrolytes were evaluated under illumination of AM1.5G simulated solar light (100 mW cm^{-2}). Figure 7a shows the $J-V$ curves with the corresponding

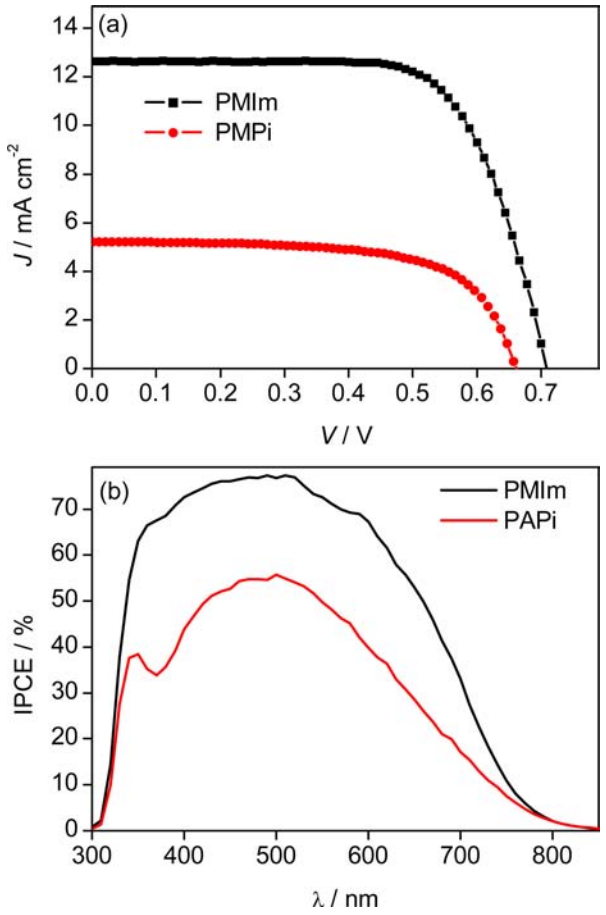

Figure 7. Photocurrent density–voltage characteristics (a) and IPCE as a function of incident wavelength (b) for ssDSSCs based on PMIm and PAPi.

photovoltaic data summarized in Table 1. PMIm produced η of 6.3% (J_{sc} = 12.65 mA cm^{-2}, V_{oc} = 0.71 V, FF = 0.70), while PMPi produced η of 2.2% (J_{sc} = 5.21 mA cm^{-2}, V_{oc} = 0.66 V, FF = 0.65). PMIm generated much higher J_{sc} than PMPi since the former has a higher conductivity than the latter. For DMPImI, which has a very low conductivity, it cannot generate photocurrent (Table 1). The obtained V_{oc} value is high considering that no 4-*tert*-butylpyridine (TBP), which is an often used additive in the electrolyte for V_{oc} improvement, is present in the device. As iodine is not included in this solid-state electrolyte, only a trace amount of triiodide exists in the device due to oxidation of iodide by oxygen in air, which is responsible for the high V_{oc}. In a DSSC system, the charge

dx.doi.org/10.1021/ja401827w | J. Am. Chem. Soc. 2013, 135, 12627–12633

recombination rate decreases with the decrease in concentration of triiodide. A slower charge recombination contributes to higher V_{oc}. Even in the absence of TBP; therefore, high V_{oc} values can be achieved using the single-component solid-state electrolyte in which no iodine is added. The value of *FF* is also impressive for ssDSSCs. The high *FF* value is the result of high conductivity for the solid-state electrolytes; higher conductivity of the solid-state electrolyte results in higher *FF* when other materials and conditions are the same. The efficiency obtained from PMIm is much higher than that obtained from spiro-MeOTAD without any additives and post-treatments[5] and is comparable to that obtained from spiro-MeOTAD with additives.[4,10]

For the MK2-based DSSC with a typical liquid electrolyte (0.6 M DMPImI, 0.1 M LiI, 0.05 M I_2, 0.5 M TBP in acetonitrile), the power conversion efficiency was 6.5% (J_{sc} = 12.76 mA cm^{-2}, V_{oc} = 0.70 V, FF = 0.73), which is comparable to that for the ssDSSC with PMIm under the same conditions. PMIm is also suitable for other dyes such as N719, which generated lower power conversion efficiency than that for MK2 by 31%.

It is impressive for an ssDSSC with a single-component solid electrolyte to achieve such high power conversion efficiency. The operation principle for the single electrolyte is the same as that for the electrolyte containing a redox couple because a trace amount of triiode or iodine is present in PMIm as revealed by the Raman (Figure S3, Supporting Information) and UV−vis (Figure S4, Supporting Information) spectra. We emphasize herein that the ssDSSCs based on these propargyl-functionalized ionic conductors work well without addition of any additives such as iodine, lithium salt, or TBP to the solid-state electrolyte. In a DSSC system, a redox couple is usually needed to reduce dye cations and accept electrons at the counter electrode. For example, the iodide alone such as LiI or DMPImI cannot operate a DSSC (Table 1) in the absence of iodine because the formed triiodide resulting from oxidation of iodide cannot transport fast enough to the counter electrode to accept the electron there due to the low conductivity, though a trace amount of iodine or triiodide is already present in the bulk electrolyte owing to oxidation of iodide. Therefore, an appropriate amount of iodine should be included in the typical electrolyte in order to complete the electric circuit. However, high photocurrent can be generated with PMIm alone as the solid-state electrolyte. This is attributed to its high conductivity; the iodide can efficiently regenerate the dye, and the triiodide can move quickly, due to efficient charge transport, to the counter electrode to accept electrons for circuit completion. Hole transfer from the dye to the ionic conductor corresponds to oxidation of iodide to I_3^-, while electron transfer from the counter electrode to the ionic conductor corresponds to reduction of I_3^- to iodide. The transfer processes of the hole and electron just look like movements of iodide and I_3^- in opposite directions. In addition, molecular interfaces between the organic dye and conductor PMIm may be well self-organized for unidirectional electron transport in the highly efficient ssDSSC.[19] For this reason, high efficiency can be achieved using this single-component solid electrolyte with high conductivity.

The influence of operating temperature on solar cell performance was also investigated in the temperature range of 30−70 °C using PMIm as the solid-state electrolyte. With temperature increasing from 30 to 70 °C, J_{sc} increased but V_{oc} decreased due to the positive shift of the conduction band with temperature.[20] The power conversion efficiency remained similar from 30 to 45 °C but decreased slightly (<10%) from 45 to 70 °C.

Figure 7b shows IPCE as a function of wavelength. IPCE values in the visible region increased in the order of PMPi < PMIm, consistent with the J_{sc} tendency for the two propargyl-functionalized ionic conductors-based ssDSSCs. The IPCE changing tendency for the two propargyl-functionalized ionic conductors is also in good correlation with the conductivity tendency. Impressively, the highest IPCE for the ssDSSC with PMIm reaches 77%, which is close to unity taking the light absorption and reflection of FTO into account. These single-component solid-state electrolytes have nearly no absorption above 400 nm, while an electrolyte containing 0.05 mM I_2 has much stronger absorption below 500 nm, as shown in Figure S4, Supporting Information. Therefore, IPCE spectra should have a difference between the DSSCs with and without iodine. Figure S6, Supporting Information, compares the IPCE spectra for the ssDSSC with the single-component solid-state electrolyte (PMIm) and the DSSC with an ionic liquid electrolyte containing 0.4 I_2 under comparable conditions. It is clear that the IPCE values ranging from 340 to 500 nm are much higher for the ssDSSC with PMIm than those for the DSSC with an ionic liquid electrolyte containing 0.4 M iodine. This indicates that the light filtering by iodine or I_3^- is successfully avoided using the single-component solid electrolyte in which no iodine is added.

The stability for the ssDSSC based on the solid electrolyte with PMIm was recorded over a period of 1500 h under 1 sun soaking (Figure 8). J_{sc} increased significantly at the beginning stage of light soaking course up to about 100 h, resulting in an increase in efficiency, as V_{oc} and FF changed slightly and

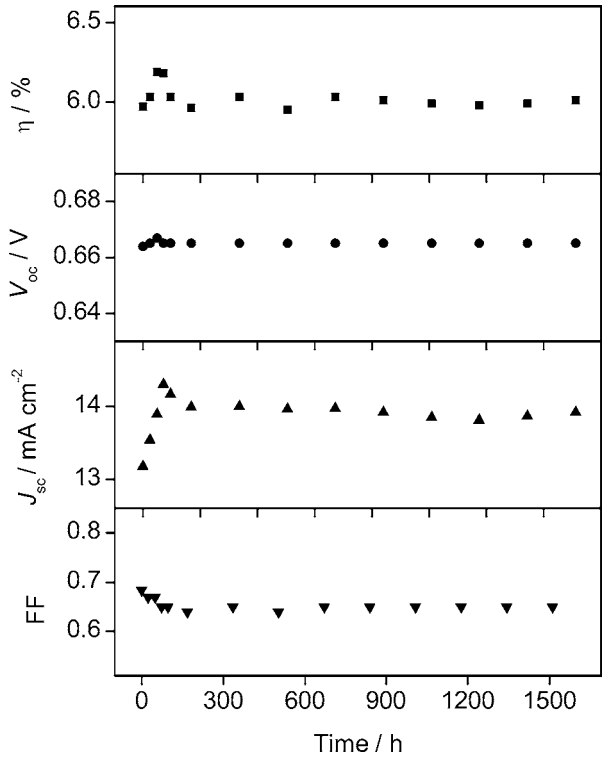

Figure 8. Evolutions of photovoltaic performance parameters under 1 sun soaking for the ssDSSC based on PMIm solid electrolyte and MK2 dye sensitizer.

dx.doi.org/10.1021/ja401827w | J. Am. Chem. Soc. 2013, 135, 12627−12633

reversely at this stage. Light soaking can increase the temperature of the device to 60 °C, which makes the solid electrolyte form a compact layer and improves the interfacial contact between TiO_2 and solid-state electrolyte. This is the plausible reason for the significantly increased J_{sc} upon light soaking up to about 100 h. Along with the increase in J_{sc}, V_{oc} increased because more electrons can lift the quasi-Fermi level of TiO_2. In the light-soaking course from 100 to 1500 h, however, all four photovoltaic parameters remained almost constant, indicating that this ssDSSC is very stable under 1 sun soaking.

■ CONCLUSIONS

In summary, novel propargyl-functionalized ionic conductors have been successfully designed and synthesized. A conductivity of 40 mS cm^{-1} at room temperature was achieved for PMIm, due to the presence of propargyl and formation of lamellar structure. As compared to the alkyl-functionalized imidazolium iodide (DMPImI), introduction of propargyl to the imidazolium ring enhanced the conductivity by more than 4-fold. The ssDSSC based on PMIm as the single-component solid-state electrolyte exhibited a power conversion efficiency as high as 6.3%. In addition, a long-term stability test demonstrated that the overall efficiency (about 6%) remained very stable during continuous light soaking for 1500 h. This discovery of high-conductivity single-component solid electrolyte paves the way for further design of new solid-state electrolytes toward high conductivity to be used in efficient and stable ssDSSCs. This finding also helps to simplify the components in the solar cell device and hence reduce the total cost.

■ ASSOCIATED CONTENT

Supporting Information

NMR spectra, dye structure, FT-IR spectra, Raman spectrum for PMIm, UV−vis absorption spectra for the solution of different electrolytes, CV curves for PMIm, and comparison of IPCE spectra. This material is available free of charge via the Internet at http://pubs.acs.org.

■ AUTHOR INFORMATION

Corresponding Author

E-mail: zs.wang@fudan.edu.cn

Notes

The authors declare no competing financial interest.

■ ACKNOWLEDGMENTS

This work was financially supported by NSFC (90922004), the National Basic Research Program (2011CB933302) of China, NSFC (20971025, 51273045), STCSM (12JC1401500), Shanghai Leading Academic Discipline Project (B108), and Jiangsu Major Program (BY2010147).

■ REFERENCES

(1) (a) O'Regan, B. C.; Grätzel, M. *Nature* **1991**, *353*, 737. (b) Gong, F.; Wang, H.; Xu, X.; Zhou, G.; Wang, Z.-S. *J. Am. Chem. Soc.* **2012**, *134*, 10953. (c) Tian, H.; Jiang, X.; Yu, Z.; Kloo, L.; Hagfeldt, A.; Sun, L. *Angew. Chem., Int. Ed.* **2010**, *49*, 7328. (d) Yella, A.; Lee, H.-W.; Tsao, H. Nok.; Yi, C.; Chandiran, A. K.; Nazeeruddin, M.; Diau, E. W.-G.; Yeh, C.-Y.; Zakeeruddin, S. M.; Grätzel, M. *Science* **2011**, *334*, 629. (e) Li, Q.; Zhao, J.; Sun, B. Q.; Lin, B. C.; Qiu, L. H.; Zhang, Y. G.; Chen, X. J.; Lu, J. M.; Yan, F. *Adv. Mater.* **2012**, *24*, 945. (f) Li, Y.; Wang, H.; Feng, Q.; Zhou, G.; Wang, Z.-S. *Energy Environ. Sci.* **2013**, *6*, 2156.

(2) (a) Kumara, G. R. A.; Okuya, M.; Murakamia, K.; Kaneko, S.; Jayaweera, V. V.; Tennakone, K. *J. Photochem. Photobiol. A* **2004**, *164*, 183. (b) Meng, Q. B.; Takahashi, K.; Zhang, X. T.; Sutanto, I.; Rao, T. N.; Sato, O.; Fujishima, A. *Langmuir* **2003**, *19*, 3572. (c) O'Regan, B. C.; Lenzmann, F.; Muis, R.; Wienke, J. *Chem. Mater.* **2002**, *14*, 5023. (d) Chung, I.; Lee, B.; He, J. Q.; Chang, R. P. H.; Kanatzidis, M. G. *Nature* **2012**, *485*, 486.

(3) Koh, J. K.; Kim, J.; Kim, B.; Kim, J. H.; Kim, E. *Adv. Mater.* **2011**, *23*, 1641.

(4) Cai, N.; Moon, S.-J.; Cevey-Ha, L.; Moehl, T.; Humphry-Baker, R.; Wang, P.; Zakeeruddin, S. M.; Grätzel, M. *Nano Lett.* **2011**, *11*, 1452.

(5) Bach, U.; Lupo, D.; Comte, P.; Moser, J.; Weissörtel, F.; Salbeck, J.; Spreitzer, H.; Grätzel, M. *Nature* **1998**, *395*, 583.

(6) Wang, G. O.; Wang, L.; Zhuo, S. P.; Fang, S. B.; Lin, Y. *Chem. Commun.* **2011**, *47*, 2700.

(7) Wu, J. H.; Hao, S. C.; Lan, Z.; Lin, J. M.; Huang, M. L.; Huang, Y. F.; Li, P. J.; Yin, S.; Sato, T. *J. Am. Chem. Soc.* **2008**, *130*, 11568.

(8) Wang, H.; Zhang, X.; Gong, F.; Zhou, G.; Wang, Z.-S. *Adv. Mater.* **2011**, *24*, 121.

(9) Martinson, A. B. F.; Hamann, T. W.; Pellin, M. J.; Hupp, J. H. *Chem.—Eur. J.* **2008**, *14*, 4458.

(10) Burschka, J.; Dualeh, A.; Kessler, F.; Baranoff, E.; Cevey-Ha, N.-L.; Yi, C.; Nazeeruddin, M. K.; Grätzel, M. *J. Am. Chem. Soc.* **2011**, *133*, 18042.

(11) Xia, J. B.; Masaki, N.; Lira-Cantu, M.; Kim, Y.; Jiang, K. J.; Yanagida, S. *J. Am. Chem. Soc.* **2008**, *130*, 1258.

(12) Jerman, I.; Jovanovski, V.; Šurca Vuk, A.; Hočevar, S. B.; Gaberšček, M.; Jesih, A.; Orel, B. *Electrochim. Acta* **2008**, *53*, 2281.

(13) Schneider, S.; Drake, G.; Hall, L.; Hawkins, T.; Rosander, M. *Z. Anorg. Allg. Chem.* **2007**, *633*, 1701.

(14) (a) Koumura, N.; Wang, Z.-S.; Mori, S.; Miyashita, M.; Suzuki, E.; Hara, K. *J. Am. Chem. Soc.* **2006**, *128*, 14256. (b) Wang, Z.-S.; Koumura, N.; Cui, Y.; Takahashi, M.; Sekiguchi, H.; Mori, A.; Kubo, T.; Furube, A.; Hara, K. *Chem. Mater.* **2008**, *20*, 3993.

(15) Wang, Z.-S.; Kawauchi, H.; Kashima, T.; Arakawa, H. *Coord. Chem. Rev.* **2004**, *248*, 1381.

(16) Wang, Z.-S.; Sayama, K.; Sugihara, H. *J. Phys. Chem. B* **2005**, *109*, 22449.

(17) Guignard, M.; Nazabal, V.; Smektala, F.; Adam, J.-L.; Bohnke, O.; Duverger, C.; Moréac, A.; Zeghlache, H.; Kudlinski, A.; Martinelli, G.; Quiquempois, Y. *Adv. Funct. Mater.* **2007**, *17*, 3284.

(18) Thorsmølle, V. K.; Rothenberger, G.; Topgaard, D.; Brauer, J. C.; Kuang, D.-B.; Zakeeruddin, S. M.; Lindman, B.; Grätzel, M.; Moser, J.-E. *ChemPhysChem* **2011**, *12*, 145.

(19) Yamanaka, N.; Kawano, R.; Kubo, W.; Masaki, N.; Kitamura, T.; Wada, Y.; Watanabe, M.; Yanagida, S. *J. Phys. Chem. B* **2007**, *111*, 4763.

(20) O'Regan, B. C.; Durrant, J. R. *J. Phys. Chem. B* **2006**, *110*, 8544.